The Astrophysical Journal, 752:151 (13pp), 2012 June 20 doi:10.1088/0004-637X/752/2/151

COLLISIONS OF POROUS CLUSTERS: A GRANULAR-MECHANICS STUDY OF COMPACTION AND FRAGMENTATION

Christian Ringl[1], Eduardo M. Bringa[2], Dalía S. Bertoldi[2], and Herbert M. Urbassek[1,3]
[1] Physics Department and Research Center OPTIMAS, University Kaiserslautern, Erwin-Schrödinger-Straße, D-67663 Kaiserslautern, Germany; urbassek@rhrk.uni-kl.de
[2] CONICET and Instituto de Ciencias Básicas, Universidad Nacional de Cuyo, Mendoza 5500, Argentina
Received 2011 August 30; accepted 2012 April 18; published 2012 June 6

ABSTRACT

The collision of granular clusters can result in a number of complex outcomes from sticking to partial or full destruction of the clusters. These outcomes will contribute to the size distribution of dust aggregates, changing their optical properties and their capability to contribute to solid-state astrochemistry. We study the collision of two clusters of equal size, formed by approximately 7000 sub-μm grains each, with a mass and velocity range that is difficult to sample in experiments. We obtain the outcome of the collision: compaction, fragmentation, and size distribution of ejecta, and type of outcome, as a function of velocity and impact parameter. We compare our results to other models and simulations, at both atomistic and continuum scales, and find some agreement together with some discrepancies. We also study collision-induced compaction as a function of cluster size, up to sizes of $N = 250{,}000$, and find that for large clusters considerably higher compactions result at higher velocities.

Key words: methods: statistical – planets and satellites: formation – protoplanetary disks

Online-only material: animations, color figures

1. INTRODUCTION

The study of impacts in astrophysics has been of interest for decades, and there is a large body of work focusing on large projectiles (0.1–10 km) (Melosh 1989). However, the universe contains a large number of dust grains, with μm and sub-μm sizes, at the interstellar and interplanetary levels, which play an important role in the evolution of the irradiated regions. For instance, interstellar dust catalyzes the formation of complex molecules, including organic molecules (Li & Greenberg 2000), and also of H_2, which determine the possible cooling and collapse of clouds into stars and planetary systems. In addition, the dust size distribution, together with its composition, determines the extinction features (Li & Greenberg 2000; Chokshi et al. 1993; Kim et al. 1994; Ormel et al. 2009). It is of interest then to study collisions between small aggregates of dust grains—we shall call them (granular) *clusters* in this work—which can change the overall size distribution, provide energy for desorbing any complex molecules which might exist on the grain surfaces, generate energy to jump chemical reaction barriers, and also modify the porosity of dust clusters, affecting the surface available for catalysis.

Experimental studies on grain–grain collisions for grains smaller than tens of μm are rare; we mention the work by Blum and coauthors on collision of individual silica grains or small agglomerates with velocities of around 1 m s^{-1} with flat surfaces (Poppe et al. 2000; Blum & Wurm 2000) and on sticking collisions leading to grain agglomeration (Wurm & Blum 1998; Krause & Blum 2004). Processes on the millimeter and centimeter scales can be roughly understood by continuum-type models. One such model of collisions, with input from experiments and numerical simulations, is the one used by Ormel et al. (2009), which is a follow-up to a series of papers by Tielens and coworkers (Chokshi et al. 1993; Tielens et al. 1994; Jones et al. 1994; Dominik et al. 1995; Dominik & Tielens 1997). These models are used to obtain the evolution of dust size distributions and the resulting absorption spectra. However, this type of model might break down at the micro-nanometer scale. To take into account some of the finer details of the dust interaction, one would need simulations incorporating complex interactions among the different components of a typical dust grain.

One strategy would be to model clusters using molecular dynamics (MD) simulations (Allen & Tildesley 1987), which solve Newton's equations of motion for an ensemble of grains interacting through an appropriate force field. Those grains themselves represent solid material which is considered unchanged internally during the collision process, while the whole ensemble—which we shall call the *cluster*—will undergo restructuring, aggregation, or fragmentation. This strategy has been used successfully to describe the collision of granular clusters containing up to several thousand grains; we mention the work by Paszun & Dominik (2009) and by Wada et al. (Wada et al. 2007, 2008; Suyama et al. 2008; Wada et al. 2009, 2011) as prominent examples.

Considerably more work has been published on the collision of *atomic clusters*, i.e., clusters of atoms, in which the motion of each individual atom is followed in the MD algorithm. We note the simulations of atomic cluster–cluster collisions with the Lennard–Jones (LJ) potential (Murad & Law 1999; Ming et al. 1997; Kalweit & Drikakis 2006; Kuninaka & Hayakawa 2009), water clusters (Svanberg et al. 1998), and metallic clusters (Mariscal et al. 2005; Ohnishi et al. 2008). Several simulations studied the collision of clusters with a surface (Tomsic et al. 2001; Kholmurodov et al. 2001; Zimmermann & Urbassek 2006; Anders et al. 2012).

Recently, Kalweit & Drikakis (2006, hereafter K&D) simulated the collision of atomic clusters containing a few thousand atoms, where the atoms interact with the LJ potential, and they determined the "phase space" for the outcomes of the collisions, as a function of relative velocity and impact parameter. Mariscal et al. (2005) studied the low-velocity collision of metallic clusters of different composition, concentrating on the degree of mixing of the components. Ohnishi et al. (2008) performed simulations similar to those by K&D, but with metallic clusters,

[3] http://www.physik.uni-kl.de/urbassek/

focusing on the resulting size distribution after the collision, and finding that a single power-law distribution did not describe their results properly.

On the other extreme, there have been many efforts to model the fragmentation of brittle (non-porous) solids using granular-mechanics techniques, often termed discrete element methods. These studies, which have been performed in two dimensions (Kun & Herrmann 1996, 1999) and three dimensions (Tong et al. 2009; Carmona et al. 2008), focus on the fragmentation behavior and the fragment size distributions. In the astrophysical context, hydrocode simulations—typically using "smoothed particle hydrodynamics" (SPH)—give detailed information on the collision and fragmentation processes of asteroids, planetesimals, and larger bodies; here also the effects of porosity could be included in the modeling (Jutzi et al. 2008). Prominent examples of simulations on aggregate collisions using this method include work by Sirono (2004), Schäfer et al. (2007), Güttler et al. (2009), and Geretshauser et al. (2010, 2011).

Models of the temporal evolution of (molecular or protoplanetary) dust clouds rely on information about the outcome of individual cluster–cluster collisions, such as they are provided here. Of special interest are data on (1) whether the two colliding clusters will stick together, forming a larger aggregate; (2) the structural and morphological changes in the aggregated cluster, which we quantify with the help of cluster compaction; and (3) the size distribution of fragments, if the collisions result in fragmentation. Cluster sizes of interest start at a few grains, but are basically unlimited in size in protoplanetary clouds, where growing clusters develop into planetesimals. Collision velocities are restricted to a few cm s^{-1} for small clusters in a protoplanetary cloud, where their motion can be described by Brownian motion in the gas disk (Weidenschilling & Cuzzi 1993; Blum 2006; Armitage 2010, 2011). However, since larger clusters tend to decouple from the gas, their relative velocities may become sizable, reaching >1 m s^{-1} for meter-sized clusters. Note that collisions with larger relative speed may occur at late times in a protoplanetary cloud, when gas (and dust) densities have decrease. Our study aims at describing collisions at relative velocities in the range $\sim$1–100 m s^{-1}. Such large velocities may also occur when shock waves, e.g., induced by a nearby supernova event, travel through a dust cloud (Draine & Salpeter 1979; Tielens et al. 1987; Ellison et al. 1997). Finally, data on collisions of small clusters might be used to extrapolate to the results of collisions of larger clusters. Actually, experimental work extends up to velocities of several m s^{-1} (Poppe et al. 2000; Güttler et al. 2010; Teiser et al. 2011), such that computational studies in this velocity range are needed.

Here we simulate the collision of granular porous clusters, each composed of up to 250,000 grains, using MD simulations. This allows us to obtain a rather complete picture of the outcome of the collision for collision velocities up to nearly 100 m s^{-1}; in particular we obtain the collision "phase space" mapping the regimes of cluster sticking and fragmentation, which allows to compare with the corresponding results for atomic clusters, and to available models. In addition, we present results on cluster compaction and of cluster fragmentation distributions. Finally, we discuss the influence of cluster size on cluster compaction.

2. METHOD

2.1. Granular-mechanics Algorithm

MD simulations (Allen & Tildesley 1987) follow the trajectories of classical interacting particles, with highly efficient numerical schemes for the integration of the equation of motion of such system. While initially used for systems composed of atoms, MD simulations soon were applied to study also the dynamics of a large collection of grains. The problems studied range from model systems (Cundall & Strack 1979) to complex macroscopic granular mechanics with technological applications (Pöschel & Schwager 2005).

State-of-the-art computer facilities could be used to simulate the dynamics of solids composed of tens of billions of atoms, following the evolution of each single atom individually (Anders et al. 2012). Using such computational resources might enable us to study the dynamical evolution of a single grain with $\sim$0.1 μm size during a fraction of a nanosecond. However, the modeling of larger grains—not to mention clusters of grains—is virtually impossible even with those resources. This also precludes the systematic evaluation of the consequences of a collision as a function of impact velocities and impact parameters as usually required. Therefore, we do not model the dynamics of individual atoms but of entire grains, neglecting the fine structure which they might possess. This appears to be a reasonable approximation for silica at the collision velocities we are simulating because plastic effects are negligible and structural phase changes are absent. This might not be the case for clusters covered with ice at the same velocities or for silica clusters at much larger velocities.

The details of our simulation method have recently been published (Ringl & Urbassek 2012). In the following, we only briefly describe the main features of our method.

Our clusters consist of spherical grains. All of them possess the same properties (radius $R_{\rm grain}$, elastic moduli, etc.). The grains only interact if the distance of their centers $d < 2R_{\rm grain}$. As common in granular mechanics, the length $\delta = 2R_{\rm grain} - d$ is called the grain *overlap*, and interactions are nonzero only for $\delta > 0$.

Forces between grains are classified as *normal* and *tangential forces*. The normal force consists of a repulsive and an adhesive contribution. The repulsive part (Pöschel & Schwager 2005),

$$f_{\rm rep} = \frac{4}{3} M \sqrt{R_{\rm red}} \delta (\delta + A v_n) \tag{1}$$

consists of a Hertzian $\delta^{3/2}$ contribution, based on elastic theory, and a dissipative part, describing a viscoelastic contact (Brilliantov et al. 1996). Here $R_{\rm red} = R_{\rm grain}/2$ is the reduced radius, $M = Y/2(1-\nu^2)$ is the reduced modulus, Y is Young's modulus, ν is Poisson's ratio, v_n is the velocity component in normal direction, and A is an empirical factor modeling dissipation. The adhesive part of the normal force is taken to be proportional to the surface energy γ (Blum 2006),

$$f_{\rm adh} = 4\pi R_{\rm red} \gamma. \tag{2}$$

Note that this value corresponds to the pull-off force needed to break a contact. We simplify the complex dependence of the adhesive force—as given by JKR theory (Johnson et al. 1971; Johnson 1985)—by a constant value (Ringl & Urbassek 2012). The tangential forces consist of several friction forces. Gliding friction,

$$f_{\rm slide} = \frac{1}{2} G \pi a^2, \tag{3}$$

depends on the shear modulus G and the radius $a = \sqrt{\delta R_{\rm red}}$ of the contact area (Burnham & Kulik 1999). Rolling motion is decelerated by a torque (Dominik & Tielens 1997, hereafter D&T):

$$D_r = 2 f_{\rm adh} \xi_{\rm yield}. \tag{4}$$

Here, $\xi_{\rm yield}$ is the distance which two grains can roll over each other without breaking their atomic contacts. Finally, also torsional motion is decelerated by a torque, whose strength is given by (Dominik & Tielens 1997)

$$D_t = \frac{1}{3} G \frac{a^3}{\pi}. \quad (5)$$

In the actual implementation, we supplement the velocity-independent friction force, Equation (3), with a velocity proportional contribution, valid for small velocities. This has the effect that the abrupt jump in the sliding force, which occurs when the tangential velocity v_t approaches zero, is smoothened. As a consequence, grain contact is stabilized. In detail, following Haff & Werner (1986) and Pöschel & Schwager (2005), we write the tangential force f_t as

$$f_t = -\mathrm{sgn}(v_t) \cdot \min\left\{\eta_{\rm tang} v_t,\, f_{\rm slide}\right\}. \quad (6)$$

The value of the damping constant $\eta_{\rm tang}$ is chosen such that the above-mentioned oscillations do not occur. The choice of $\eta_{\rm tang}$ thus depends on the adopted time step, Δt, and is best determined by a test simulation. We found a value of $\eta_{\rm tang} = 0.1 m/\Delta t$ appropriate. For the other friction forces we proceed analogously. For details see Ringl & Urbassek (2012).

Our simulations have been performed with the well-documented MD package LAMMPS[4] (Plimpton 1995) after the above features have been coded into this software. We explicitly note that features like rigid-body rotation or the exertion of torques by tangential forces—which are not common in atomistic simulation—are correctly implemented in this software.

2.2. Parameter Selection

The materials parameters are chosen as appropriate for SiO_2 (Chokshi et al. 1993): Young's modulus $Y = 54$ GPa, Poisson's ratio $\nu = 0.17$, shear modulus $G = Y/[2(1+\nu)]$, and $\gamma = 0.05$ Jm^{-2} is twice the surface energy of SiO_2. The constant A, Equation (1), was fitted to the measured typical value (Poppe et al. 2000), of the restitution coefficient ($\epsilon = 0.69$) of two spheres at a relative velocity of 1 m s^{-1}; this yields $A = 0.5 \times 10^{-9}$ s. We note that in our model ϵ is velocity dependent (Ringl & Urbassek 2012), similar to available theories (Thornton & Ning 1998) and experiment. Finally, the distance $\xi_{\rm yield}$ needed to calculate rolling friction was set to 10^{-10} m (Dominik & Tielens 1997).

While these above parameters are quite routinely used to describe small silica grains, the possible occurrence of plasticity in the individual silica grains needs further discussion. A granular-mechanics approach of collisions presupposes that individual grains will not deform plastically under the collisions. The yield strength of (macroscopic) silica is only a fraction of the ideal yield strength of defect-free single-crystalline silica, which can be estimated to $J_0 \sim Y/5$ (Chokshi et al. 1993). However, in small grains dislocations are not free to develop and multiply (Hall–Petch effect) (Meyers & Chawla 2010), which increases significantly their yield strength. In addition, it is known that the strength of most materials increases with strain rate (Murphy et al. 2010); since the strain rates encountered in our granular collisions reach $\sim 10^9$ s^{-1}, we can assume that the yield strength in our system is close to the ideal strength, J_0. Indeed shock experiments measure the Hugoniot elastic limit of amorphous silica to be around 6–9 GPa (Rosenberg et al. 1996). We may use the estimate of Thornton & Ning (1998) to calculate the critical velocity above which plasticity sets in,

$$v_{\rm plast} = 3.19 \left(\frac{2^5 J^5 R_{\rm red}^3}{M^4 m}\right)^{1/2}, \quad (7)$$

where m is the mass of a grain. We obtain $v_{\rm plast} = 250$ (690) m s^{-1} for the experimental values of $J = 6$ (9) GPa. An estimate based on Equation (33) of Chokshi et al. (1993) gives similar numbers (Ringl & Urbassek 2012). We conclude that plastic effects can be safely ignored in the range of velocities considered in the present work.

2.3. System and Simulation

We first focus on the collision of two clusters containing $N = 7200$ grains each. The grain radius was kept fixed as $R_{\rm grain} = 0.76\,\mu$m. The density of the SiO_2 grains amounts to $\rho = 2 \times 10^3$ kg m^{-3} (Blum & Schräpler 2004).

We construct the spherical clusters by adding randomly grains to a central grain with the constraint of keeping the average filling factor at a predefined value. The filling factor of the clusters is measured locally as the density around a grain in a sphere of radius $5R_{\rm grain}$. The *global* filling factor ϕ is the average over the local filling factors. The filling factor of our clusters has be chosen as a typical value for dust aggregates in space, $\phi = 20.5\%$. The radius of our clusters was kept fixed at $R = 28\,\mu$m.

The clusters collide with relative velocities v varying between 1 and 85 m s^{-1}, and with impact parameters b varying between $b = 0$ (central collision) to $b = 0.9R$. Our study is hence focused on head-on or nearly head-on collisions. We did not perform simulations for larger values of b (more peripheral collisions) since then only few grains participate in the collision and the compaction will be drastically reduced. In our series of simulations, only the relative cluster velocity, v, and the impact parameter, b, vary.

In order to provide some statistics, for each set of v and b, we average over eight individual collision events; these differ from each other by random rotation of the clusters. We tested that eight rotations are enough to give us a statistically meaningful data set. We simulate for a time of 10^{-4} s. Since we employ a simulation time step of 50 ps, we thus integrate our equations of motion over 2×10^6 time steps. The time step is short enough to ensure proper integration of the equations of motion (Ringl & Urbassek 2012), and the total simulated time is long enough for the collisions to provide the final, unchanging, size distributions, and filling factors for the resulting fragments.

We employ a cubic simulation box with a side length of 5×10^{-4} m and periodic boundary conditions. The box size is large enough to minimize possible boundary condition artifacts.

2.4. Fragmentation and Sound Velocities

For comparison with available models and other computational studies, it is useful to introduce two characteristic velocities of our system.

The *fragmentation velocity* $v_{\rm frag}$ is defined as the smallest velocity, which a bound pair of grains needs to be imparted for dissociation. This is easily calculated in a simulation involving only two grains. We find $v_{\rm frag} = 0.17$ m s^{-1}. This velocity corresponds to an energy

$$E_{\rm break} = \frac{m}{4} v_{\rm frag}^2 = 2.66 \times 10^{-17}\ \mathrm{J} \quad (8)$$

[4] http://lammps.sandia.gov

in the center-of-mass system of the two grains involved. This energy has been called the *break-up energy* by Dominik & Tielens (1997), since it characterizes the minimum energy necessary to break a contact.

This fragmentation velocity is about a factor of five smaller than that found in experiments performed by Poppe et al. (2000) on μm-sized silica spheres ($\sim$1 m s^{-1}). However, our velocity fits well with what is known from analytical work (Chokshi et al. 1993). We surmise that differences may originate from the model character or our simulation (ideal spheres, monodisperse sizes, etc.) while for realistic grains, e.g., surface imperfections and roughness will enhance the fragmentation velocity.

Collision velocities of atomic clusters are often related to the sound speed in that material. Thus, for collisions of LJ clusters, such as in Kalweit & Drikakis (2006), the LJ velocity of sound (Ashcroft & Mermin 1976; Quesnel et al. 1993),

$$v_{\rm sound}^{\rm LJ} = \sqrt{\frac{B}{\rho}} = \sqrt{\frac{75\varepsilon/\sigma^3}{4\times 1.05 m/\sigma^3}} = 4.23\sqrt{\frac{\varepsilon}{m}}, \qquad (9)$$

is employed, where ε and σ are the usual LJ parameters, m is the atom mass, B is the bulk modulus of an fcc LJ crystal, and ρ is its density.

For the case of our granular clusters, we use the model presented by Paszun & Dominik (2008):

$$v_{\rm sound} = \left(1-\frac{2}{n_c}\right)(2R_{\rm grain}-\delta_{\rm equ})\sqrt{\frac{6\gamma}{R_{\rm grain}^3\rho}} = 19.86\ {\rm m\,s^{-1}}, \qquad (10)$$

where $n_c/2 = 7475$ is the number of contacts in one cluster, and the equilibrium overlap $\delta_{\rm equ}$ is given by

$$\delta_{\rm equ} = \left(\frac{9\pi^2\gamma^2 R_{\rm red}}{M^2}\right)^{1/3} = 3.0\times 10^{-10}\ {\rm m}. \qquad (11)$$

We note that these two last equations contained a typo in our recent publication (Ringl & Urbassek 2012). In that reference we also showed that our code gives sound speeds for granular material in good agreement with available theoretical estimates (Paszun & Dominik 2008).

3. RESULTS

3.1. Agglomeration and Fragmentation

Figure 1 displays snapshots (generated by VMD; Humphrey et al. 1996) to show the dynamics of a cluster–cluster collision. The two clusters shear material off each other and are decelerated during this process. Consequently they stick to each other at their interface, while the far ends of the clusters continue moving onward. The friction process leads to *evaporation* of single grains of the cluster starting at the interface but continuing all over the two clusters' surfaces. Due to the non-zero impact parameter, a torque is exerted on the system leading to rotation. In the final stage, the two clusters have merged at the interface, forming a composite central cluster, containing roughly one-third of the entire mass. Note that the interface remains clearly visible in this cluster with only little intermixing. The original clusters still survive to some extent leading to two more large clusters; the largest of these surviving clusters contains 5537 grains. These clusters are almost pure, containing only material

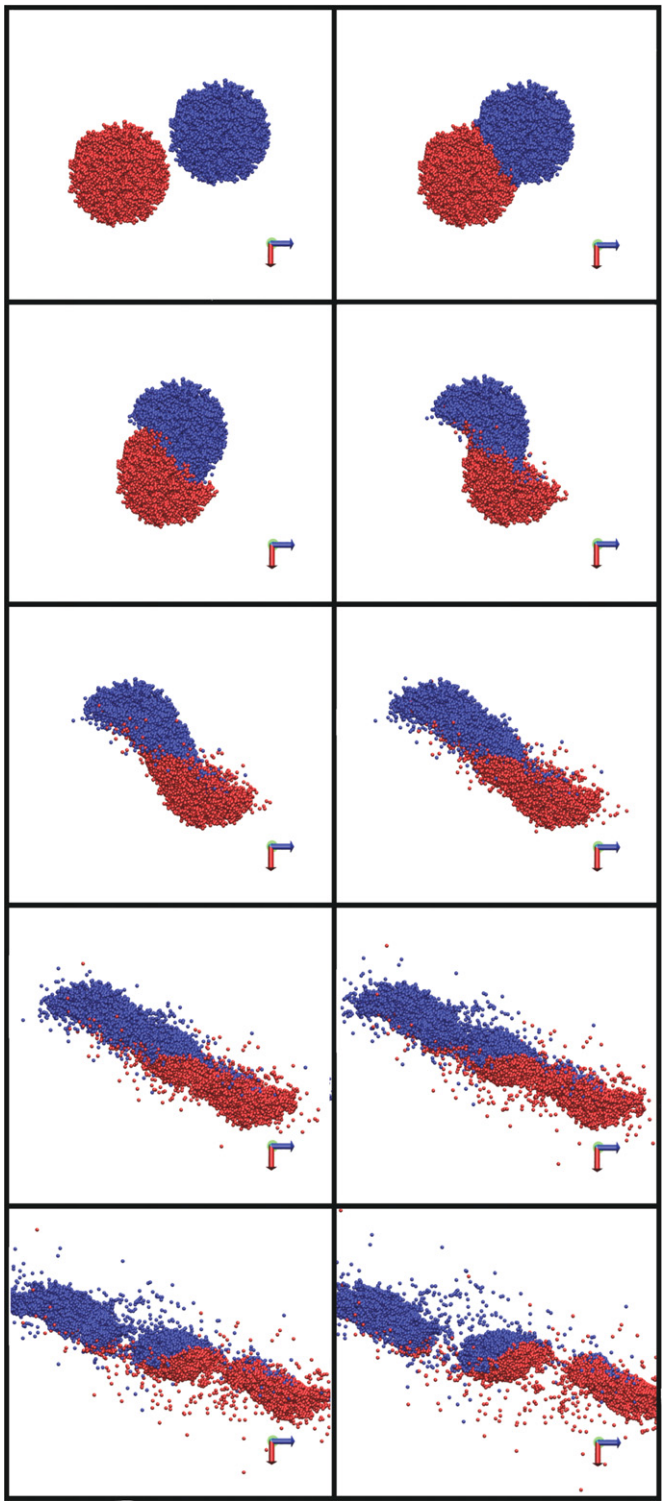

Figure 1. Time series of a cluster–cluster collision, snapshots taken every 5 μs. Color differentiates the original cluster to which a grain belongs. Center-of-mass frame. Velocity $v = 5$ m s^{-1} ($v = 29 v_{\rm frag}$) and impact parameter $b = 0.8$ R were selected.

of their mother cluster; only a few percent of grains of the collision partner have been incorporated to their surface. Besides these three large clusters, a cloud of *evaporated* grains surrounds them.

This sequence of events and the final outcome are strongly reminiscent of atomic cluster collisions, as studied by MD simulations (Kalweit & Drikakis 2006; Ohnishi et al. 2008).

However, the small amount of intermixing found for granular clusters is a feature which contrasts with the mixing found for metallic clusters (Mariscal et al. 2005). We note that the rapid cooling of the granular system prevents thermal intermixing to occur at later times. The collision and fragmentation behavior is also reminiscent of simulations describing the collision of satellites, as in the work of Asphaug et al. (2006) using SPH simulations.

The scenario depicted in Figure 1 can be characterized as a partial fragmentation. Depending on the cluster velocity and impact parameter, quite distinct scenarios can exist. Figure 2 shows representative snapshots taken at the end of the simulation time for the main scenarios we have found.

1. Agglomeration: for small velocities and not-too-large impact parameters the two clusters will fuse forming one big cluster.
2. At higher velocities and/or larger impact parameters, multifragmentation occurs. This encompasses the case shown in Figure 1, but the number of multi-grain fragments will generally be larger than three.
3. For even higher velocities cluster destruction will be the dominating process.

In all these cases the surviving clusters are surrounded by a cloud of evaporated grains.

The merged cluster shown in Figure 2 has a roughly spherical shape; this occurs at this particular choice of impact parameter. For central collisions, the original form of the individual clusters tends to survive leading to a final elongated cluster, and the more so at low collision velocities (cf. Figure 3).

Figure 4 presents the delineation between these three different scenarios in a more systematic way, viz. as a function of impact parameter and velocity. This plot is based on a quantification of the amount of cluster destruction (cf. Kalweit & Drikakis 2006),

$$N_s = 1 - \frac{N_1 + N_2}{2N}, \tag{12}$$

where N_1 and N_2 denote the number of grains in the two largest clusters found at the end of the simulation. Evidently, both for elastic scattering and for cluster agglomeration, $N_s = 0$, while for multifragmentation or complete cluster fragmentation $N_s \to 1$.

The plot quantifies how with increasing velocity and impact parameter, agglomeration ceases, and fragmentation becomes dominating. In addition the different regimes have been indicated in the plot. To this end, in agreement with Kalweit & Drikakis (2006), we define the quantity

$$X = \frac{N_1 - N_2}{2N}. \tag{13}$$

If $X > 0.15$, the collision result is classified as "sticking," and otherwise as "fragmentation" (Kalweit & Drikakis 2006).

3.2. Comparison with Atomistic Models

Several collision modes have been identified for collisions of atomic clusters. A prominent example is given in the work by K&D on LJ clusters (Kalweit & Drikakis 2006). Their results have been included in Figure 4 in the form of lines bounding different collision regimes. (The fits are of an exponential form, $N_s = a\exp(-x/b) + c$, where $x = v/v_{\rm sound}^{\rm LJ}$. We use for the green line $A = 18.8$, $b = 0.12$, $c = 0.11$, and for the blue line $a = 2.46$, $b = 0.37$, $c = 0.07$.) The area under the

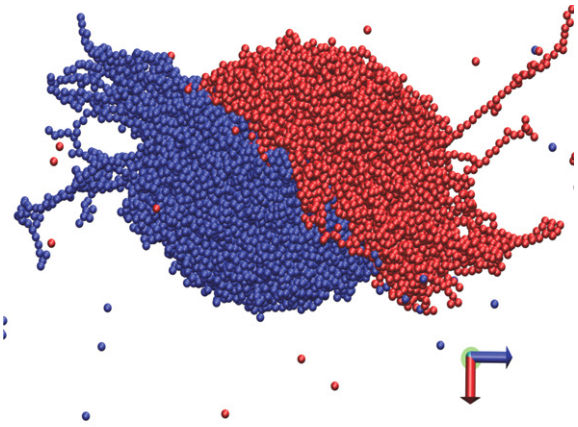

(a)

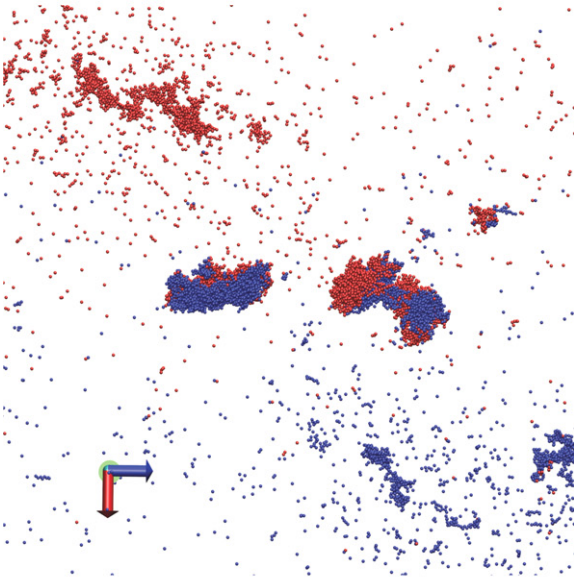

(b)

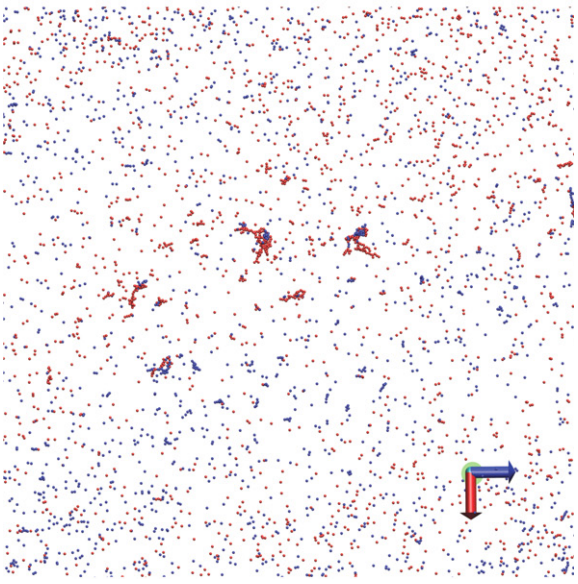

(c)

Figure 2. Final snapshots for different collision events showing the regimes of agglomeration, partial, and total fragmentation. (a) $v = 2$ m s^{-1} ($v = 12v_{\rm frag}$); (b) $v = 5$ m s^{-1} ($v = 59v_{\rm frag}$); and (c) $v = 10$ m s^{-1} ($v = 176v_{\rm frag}$). In all cases, the impact parameter was selected to be $b = 0.6R$.

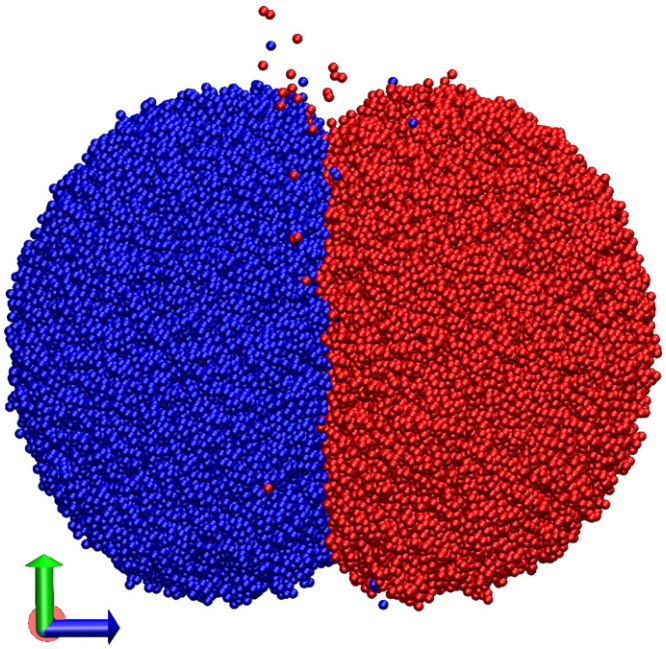

Figure 3. Final snapshots showing the agglomeration of two clusters of $N = 57{,}000$ grains each. A central collision with a velocity of $v = 1$ m s^{-1} ($v = 6v_{\rm frag}$) is shown. Color differentiates to which cluster the grains originally belonged. The original form of the clusters is better conserved than in Figure 2(a).

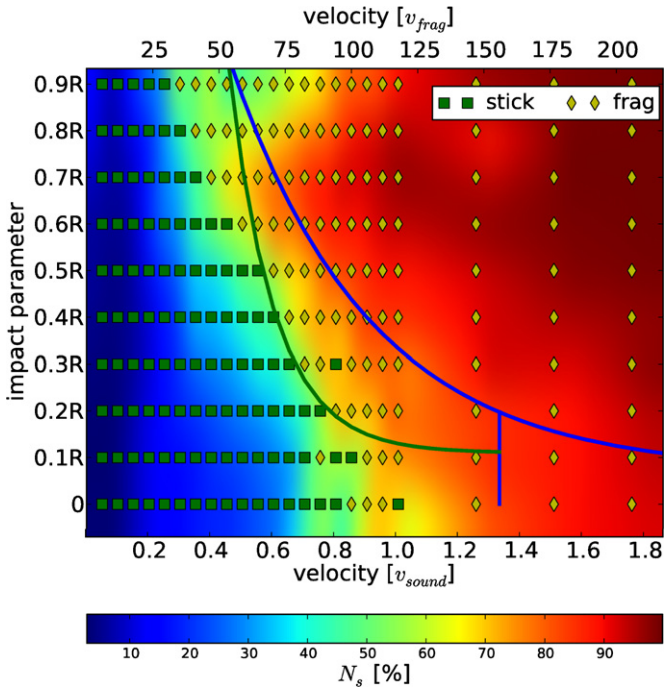

Figure 4. Color: cluster fragmentation quantified by N_s, Equation (12). In addition, the different regimes of *sticking* and *fragmentation* according to the criterion of $X > 0.15$ or $X < 0.15$, Equation (13), are indicated by the symbols. The lines delineate the results found in a previous study of LJ-cluster collisions (Kalweit & Drikakis 2006); see the text.

green curve is the sticking region, where the collision results in both clusters sticking together, while their internal structures remain intact. In the stretching–separation mode, the area above the blue curve fit, clusters collide and separate into two main fragments and additional satellite fragments. The area between the green and blue curves represents the so-called slide-and-locking mode, which forms a transition region between sticking and stretching–separation mode. Finally, the area above the blue curve fit and $v/v_{\rm sound} > 1.1$ indicates the droplet mode, where the high impact energy results in one main fragment in a disordered phase and significant scattering and evaporation.

The agreement between our results and those of the atomistic simulation in the regions determining the collision outcome is striking, despite the large differences in scale and between atom–atom/grain–grain interaction details. We do note that collisions between atomic clusters typically lead to extremely hot ejecta, with melting of the fragments. This is not the case here, where individual grains do not have internal degrees of freedom like vibrations, and dissipation rapidly cools the fragments. The limitations of our model would preclude its useful utilization at much larger velocities, where solid–solid and solid–liquid phase transitions might play important roles.

3.3. Compaction

Due to the collision process, the porous clusters will compactify. We measure compaction with the help of the filling factor ϕ. The data are assembled in Figure 5 and Figure 6. Initially the clusters have filling factors of 20.5%. For small velocities, up to $v \lesssim 25v_{\rm frag}$, the filling factor increases monotonically with velocity. It is maximum for central collisions, while less compaction is achieved for more peripheral collisions (cf. Figure 6). We observe a maximum compaction of $\phi = 37.5\%$ for central collisions at a velocity of $v = 26v_{\rm frag}$. Note that the compaction process occurs entirely in the agglomeration regime.

Analyzing Figure 6 qualitatively, one could argue that at very low velocities there is little compaction, and therefore there will be almost no impact parameter dependence. At high velocities, there is significant fragmentation and therefore compaction is again nearly independent of impact parameter. For intermediate velocities, one might expect that compaction would depend on the overlap geometry of the colliding clusters, which depends on b^3. This is not the case, and further simulations and modeling are needed to understand this dependence.

Beyond this velocity, the filling factor decreases again. This is not astonishing at higher velocities, in the multi-fragmentation regime, which holds for central collisions for $v \gtrsim 100v_{\rm frag}$. However, the decline in compaction occurs already at much smaller velocities, $v \gtrsim 25v_{\rm frag}$. We explain this feature with the help of Figure 7. Here the result of central collisions in the agglomeration regime with velocities $v = 29v_{\rm frag}$ and $59v_{\rm frag}$ are depicted. In both cases, the resulting cluster has been considerably squeezed in the collision direction and thus strongly deviates from its spherical shape. The pancake shape assumed explains the high compactions in the central region (see bottom row figures). However, the agglomerated cluster expands laterally from the collision zone and thus has a means to relax stresses and withstand compaction. Thus, in contrast to collisions of stiff porous media (like metallic foams) or of laterally strongly extended (broad) impactors, this figure shows that lateral cluster deformation is an efficient means to avoid compaction.

Compaction of porous clusters by collisions was measured recently by Teiser et al. (2011). They observed increasing compaction up to their highest collision velocities if 8 m s^{-1}. This is, however, not in contradiction to our results, since their velocities are still relatively small. Moreover they use large clusters, of the order of 100 μm in size; as we shall show below, in Section 3.4, compaction is increased for large clusters at

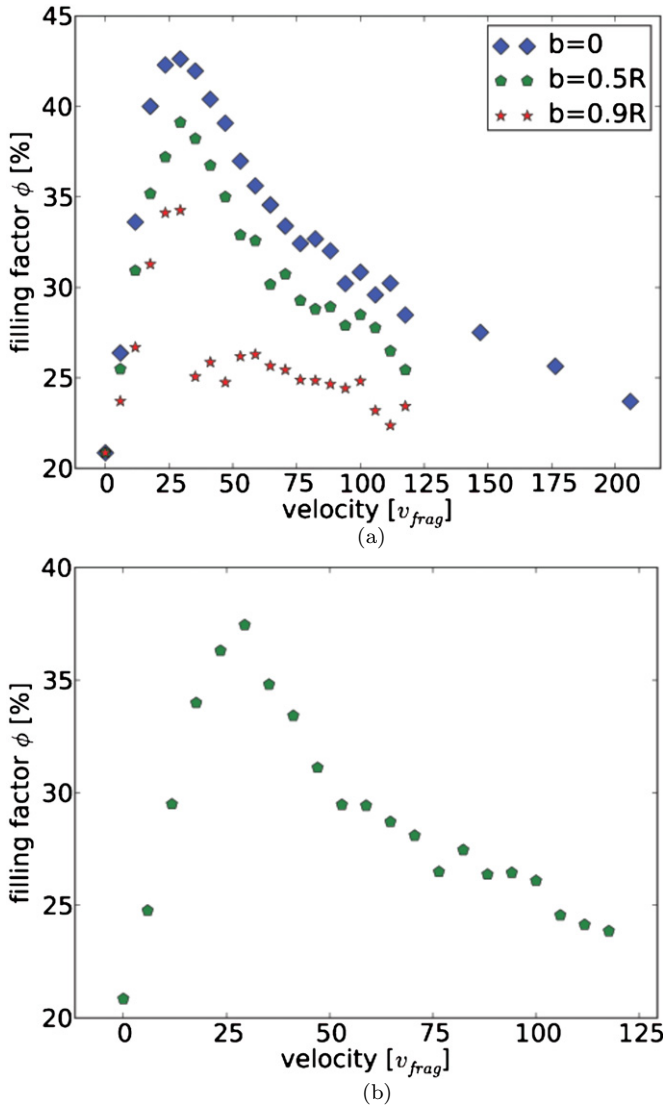

Figure 5. Filling factor as a function of velocity (a) for several impact parameters b and (b) averaged over the impact parameter b.

(A color version of this figure is available in the online journal.)

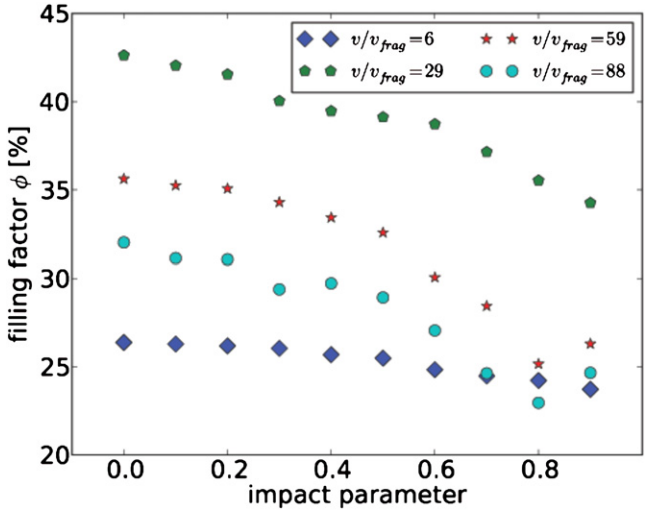

Figure 6. Filling factor as a function the impact parameter b for various velocities v.

(A color version of this figure is available in the online journal.)

higher velocities. The reason is that in larger clusters, the effect of lateral expansion to reduce the compaction of the core will be less efficient. We conclude that it would be interesting to extend the measurements by Teiser et al. to higher velocities, where our simulations predict a leveling off of the collision-induced compaction.

The compaction plots in Figure 7 demonstrate that filling factors tend to be maximum in the interior of the aggregated cluster, and decrease toward the surface. This latter effect is a result of the detector, which measures the local density by counting the grains inside a sphere of radius $5R_{\rm grain}$; see Section 2. More interestingly, however, is the fact that the filling factor is quite heterogeneous also inside the cluster. This is of course the consequence of the random nature of the initial cluster structure. Note that for $v = 29v_{\rm frag}$, close to the compaction maximum, local filling factors reach up to 60%. For the higher velocity, $v = 59v_{\rm frag}$, filling factors up to 50% still can be observed. We observe in Figure 7(d) how a small part of the aggregated cluster seems to be almost separated from the main body of the cluster (discernible by the horizontal green line), indicating a high porosity connection with the main part of the aggregated cluster. This is an example of a general finding observed in our simulations; fragmentation starts at the periphery of the aggregated clusters, far from the collision axis.

We note that global compaction estimates in Figure 6 have to be taken with care for collisions at this scale. Our results for a "local" filling factor point at the complexity of the problem. For instance, as shown in Figure 7, we could find large compaction at the core of a grain, while the outer layers are not highly compacted, maintaining their potential for catalysis.

Paszun & Dominik (2009) studied compaction with clusters containing 1000 grains. For central collisions, they find an increase of the global filling factor; beyond the maximum compaction, they also see a decline of compaction toward higher velocities. They ascribe this effect to the flattening—as a geometrical effect—of the merged cluster. While we also see this flattening (cf. Figure 7) our interpretation is dynamic, not geometric: the lateral cluster expansion relaxes the density increase in the center and thus leads to less compaction. In addition, our studies on larger clusters (see Section 3.4 below) demonstrate that this effect diminishes with increasing cluster size.

Wada et al. (2008) measure compression with the help of the radius of gyration—a rather global criterion. They find that compaction increases with impact velocity, up to a maximum; the decrease of compaction beyond that maximum is interpreted as a disruption effect.

3.4. Results for Larger Clusters

The efficient performance of our code also allows us to study the result of collisions of larger clusters. In Figure 8, we study how collision-induced compaction depends on cluster size. In addition to the size $N = 7200$ studied until now, we also consider $N = 57{,}000$ and $N = 250{,}000$. Only central collisions (impact factor $b = 0$), which maximized compaction, were simulated, and for the largest cluster only five events were calculated.

We observe that the velocity dependence of the larger clusters overall is analogous to the smaller clusters, exhibiting a maximum in compression at velocities of around $(20 \ldots 40)v_{\rm frag}$. In detail, however, the following trends become visible.

1. The velocity at which the maximum compression occurs increases with increasing cluster size.

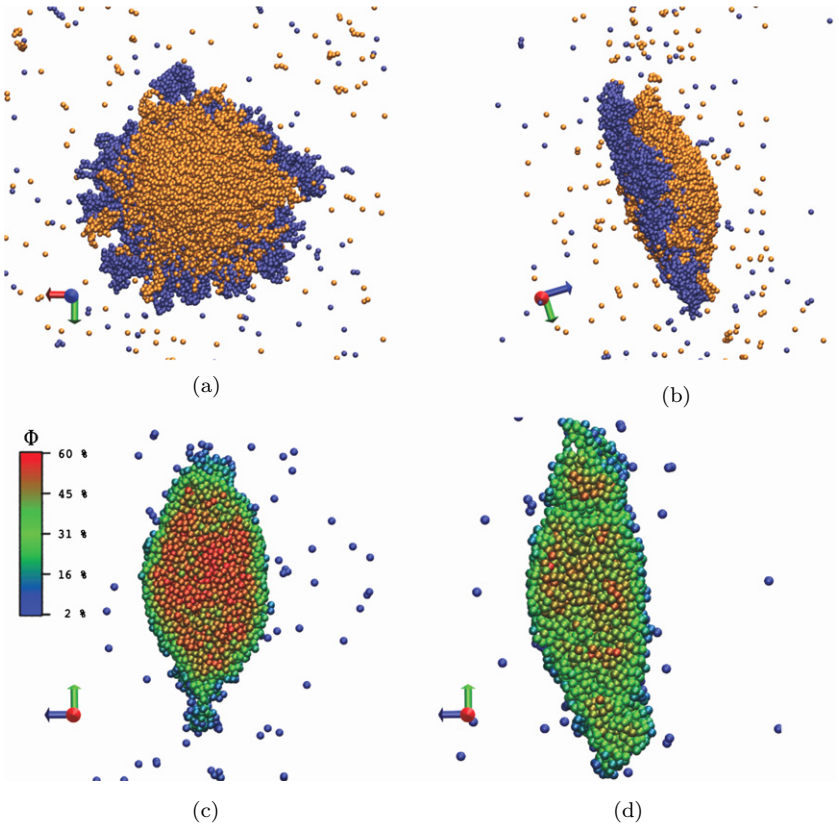

Figure 7. Effect of velocity on cluster deformation (top) and local filling factor (bottom): left: $v = 29v_{\rm frag}$; right $v = 59v_{\rm frag}$. The colors in the top row indicate the initial clusters, and in the bottom row the filling factor. Both collisions were central ($b = 0$). Snapshots taken at the end of the simulation.

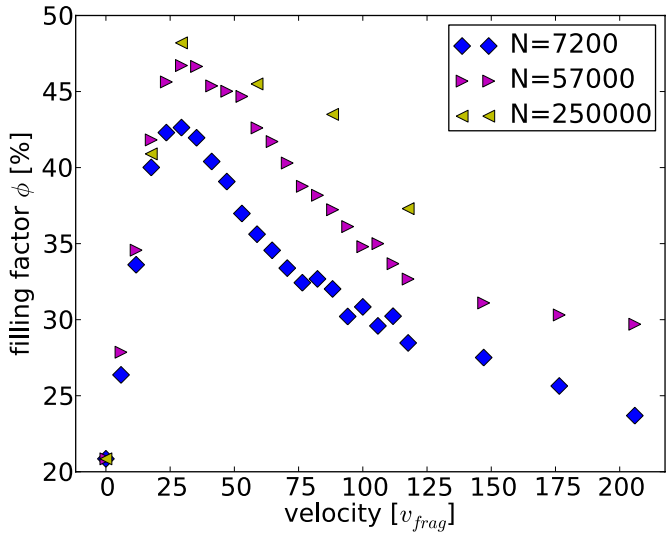

Figure 8. Filling factor as a function of velocity for central collisions (impact parameter $b = 0$) for various cluster sizes N.

2. The maximum achievable compression increases with cluster size.
3. While only a narrow velocity window led to maximum compression for the smallest cluster, $N = 7200$, the velocity window broadens with increasing cluster size. Thus, on the high-velocity side, the influence of cluster size on compaction is most sizable.

All these features are understandable from the collision dynamics of clusters. With increasing size, clusters behave more like bulk material; the possibility of relaxing the pressure and compaction sideways—which was clearly seen in the pancake-shaped clusters of Figure 7—becomes less efficient. Therefore, the tendency for compaction also remains for higher velocities, leading both to the shift of the maximum to higher velocities and to a higher achievable compaction.

The resulting cluster shapes and local compactions are displayed in Figure 9. We observe that compaction is now quite homogeneous in the resulting cluster. Figures 9(c) and (d) also help us to understand why compaction remains large in large-cluster collisions at high speeds ($88v_{\rm frag}$): the resulting merged cluster still appears homogeneously "baked together" and the tendency toward cluster fragmentation is apparently low. Compare this with the small-cluster result, Figure 7(d), at a lower velocity ($59v_{\rm frag}$): here the shape has already become quite irregular, and a smaller overall compaction has been achieved. The details of the collision dynamics can be observed in the animations in the online journal accompanying Figure 9.

3.5. Comparison with Analytic Models

D&T provided a model of granular cluster collisions which is often used in planetary sciences, including in recent papers by Ormel and coworkers (Ormel et al. 2009; Güttler et al. 2010; Zsom et al. 2010). We present a brief summary of three relevant quantities: (1) the minimum energy needed for restructuring the cluster, (2) the energy needed for maximum compaction, and (3) the energy needed for fragmenting the cluster.

1. D&T discuss cluster restructuring using the so-called *rolling* energy ($E_{\rm roll}$), which they define as the energy required to roll the contact area between two grains a distance $\pi R_{\rm red}$, i.e., two spheres roll by 90° over each other. This

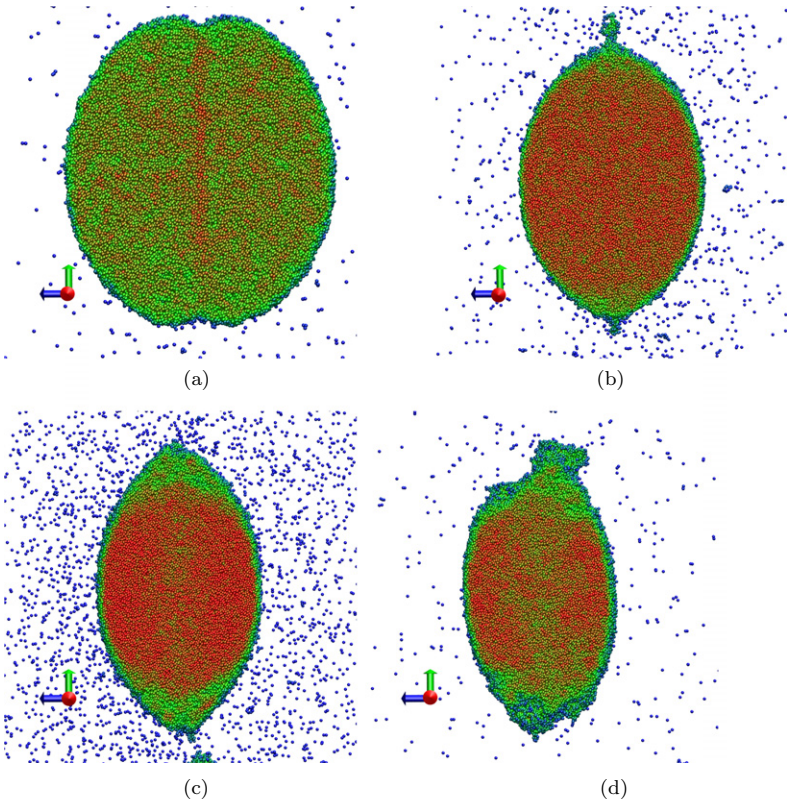

Figure 9. Effect of velocity on local filling factor for clusters containing $N = 250{,}000$ grains. Collision velocities (a) $v = 17.6 v_{\rm frag}$, (b) $v = 29 v_{\rm frag}$, (c) $v = 59 v_{\rm frag}$, and (d) $v = 88 v_{\rm frag}$. Colors indicate the filling factor as in Figure 7. Collisions were central ($b = 0$). Snapshots taken at end of simulation.

(Animations of this figure are available in the online journal.)

energy is

$$E_{\rm roll} = 6\pi^2 \xi_{\rm yield} \gamma R_{\rm red} = 1.125 \times 10^{-16}\,{\rm J}. \quad (14)$$

When collisional energies are low enough for cluster restructuring to be important ($E \lesssim 5E_{\rm roll}$), clusters are in the *sticking-without-restructuring regime*. This occurs at very low speeds, when $v/v_{\rm sound} < 3.8 \times 10^{-4}$ (using $\xi_{\rm yield} = 0.1$ nm). Therefore, in our simulations, collisions are strong enough to easily modify the initial morphology of the clusters.

We note that the value of $\xi_{\rm yield}$, which enters this expression, has been set to 0.1 nm, as in the original work by D&T. Following laboratory experiments (Blum & Wurm 2000) other authors use the value $\xi_{\rm yield} = 2$ nm (Ormel et al. 2009), for which $E_{\rm roll} = 2.25 \times 10^{-15}$ J; then cluster restructuring starts at $v/v_{\rm sound} < 1.7 \times 10^{-3}$. Either of these limits is in agreement with our simulation results.

2. D&T find that *maximum compression*—in our wording: compaction—of the clusters occurs when the collision energy, E, is equal to $n_c E_{\rm roll}$. For our SiO_2 clusters, $n_c = 14950$ (14950/2 per cluster), and the collision energy is related to the relative velocity v and the mass m of a cluster by

$$E = \frac{m}{4} v^2. \quad (15)$$

D&T thus predict maximum compaction for $v/v_{\rm sound} = 0.02$ ($v/v_{\rm frag} = 2.9$). This is obviously a strong underestimation of our simulation results, Figure 5 and Figure 6, which give maximum compaction at $v/v_{\rm frag} = 26$. Even with the more recent value of $\xi_{\rm yield} = 2$ nm, the D&T prediction only becomes $v/v_{\rm sound} = 0.09$ ($v/v_{\rm frag} = 13$). We must conclude that the large clusters studied by us do not fulfill the D&T predictions, which are based on an extrapolation from their simulations with cluster sizes <100 grains.

Ormel et al. (2009) found a maximum in the filling factor when the collision energy was nearly $0.2 n_c E_{\rm roll}$ for head-on collisions and about $n_c E_{\rm roll}$ for glancing collisions. This corresponds to a collision energy of (1.7–8.4) $\times 10^{-13}$ J using the $E_{\rm roll}$ from D&T, and (6.7–33) $\times 10^{-12}$ J using the $E_{\rm roll}$ from Ormel et al. (2009). However, this maximum corresponds to roughly maintaining the same compaction, and a decrease of up to 30% is found elsewhere in the simulated range. Larger filling is only attained for larger initial porosities. For both head-on and glancing collisions, the energy at which a maximum filling is reached in our simulations is found at $v/v_{\rm frag} \approx 25$, giving an energy of 1.2×10^{-10} J. In our simulations the maximum persists even at large impact parameters, while it flattens out in the simulations in Ormel et al. (2009).

3. At larger energies, D&T call the outcome of the collision a *catastrophic disruption* if the impact breaks at least half of the bonds between the individual grains. The energy needed to produce this phenomenon is a factor $10 n_c$ higher than the energy to break a single bond, $E_{\rm break}$, because a large energy fraction goes to kinetic energy of the fragments. Therefore, catastrophic disruption occurs when $E > 10 n_c E_{\rm break}$ according to their simulations of small clusters. In their model D&T find

$$E_{\rm break} = K \frac{\gamma^{5/3} R_{\rm red}^{4/3}}{M^{2/3}}, \quad (16)$$

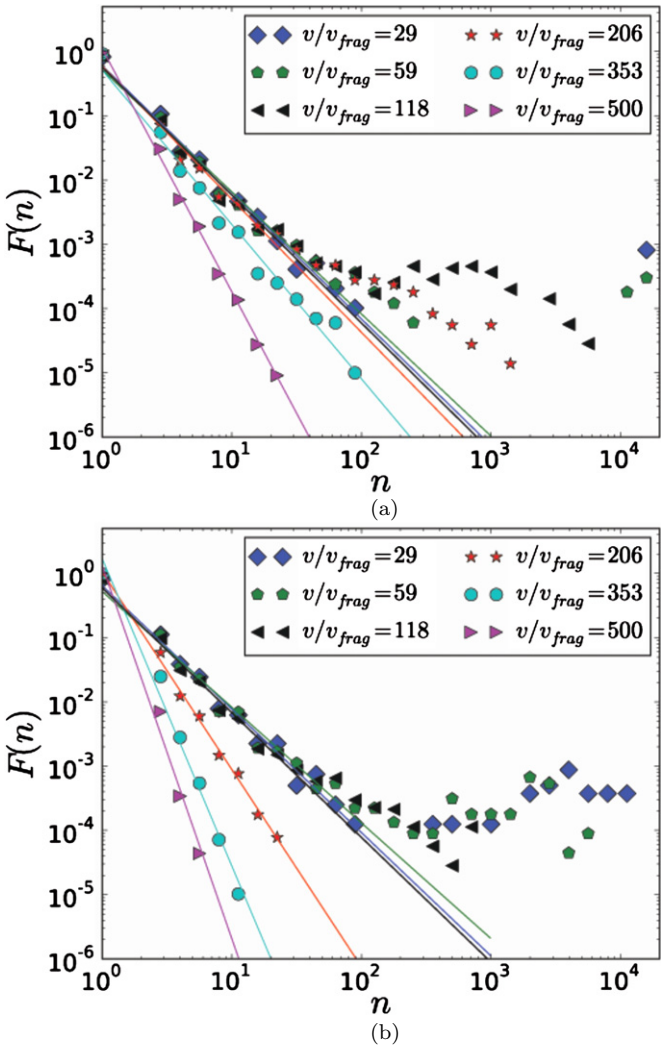

Figure 10. Fragment distributions for (a) central ($b = 0$) and (b) more peripheral ($b = 0.8R$) collisions. The lines give fits to power-law distributions; see the text.

(A color version of this figure is available in the online journal.)

where K is a dimensionless constant. D&T find $K = 43$ when vibrations are included, and $K = 2.1$ when only a simple continuum elastic model of adhesion is used. From our simulations, we can easily determine $K = 13$, based on the velocity needed to separate a dimer; see Equation (8). We explain this discrepancy by noting that our model includes dissipation, and hence K should be increased compared with the purely elastic value; since, however, vibrations within a grain are not included, our value is smaller than the D&T value of $K = 43$. On the other hand, Ormel et al. adopted the factor $K = 2.8 \times 10^3$ from experimental data (Blum & Wurm 2000). We note that all experiments used by Ormel are from a region of cluster size and velocity far from those studied here.

According to D&T, we should get catastrophic disruption when $v/v_{\rm sound} > 0.03$ (using $K = 13$), while in the simulations this happens for $v/v_{\rm sound} \gtrsim 1.1$. This disagreement is severe and is likely due to the simplifying assumptions in the mechanics of fragmentation in D&T, given that the energy to break the contact between grains is only off between the models by a factor of three to four, providing another example where extrapolations at the micro-nano size scale can be problematic. We note that

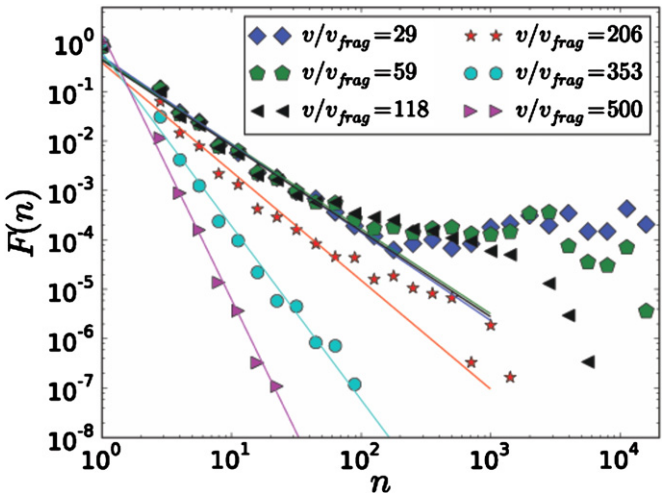

Figure 11. Fragment distributions, averaged over impact parameter b, for various velocities.

(A color version of this figure is available in the online journal.)

our simulation result can be accommodated in the D&T model by fitting the constant K in Equation (16) to $K = 520$; this is, however, unsatisfactory since the breakup energy is directly accessible to simulation and gives $K = 13$.

A recent compilation by Güttler et al. (2010) reviews experimental data on the critical velocity of equal-mass silica clusters and reports a value of 1 m s^{-1}. However, earlier experiments by Wurm et al. (2005) and Teiser & Wurm (2009) report cluster growth at velocities >13 m s^{-1}. Our results give a critical velocity around $100v_{\rm frag} = 17$ m s^{-1} (cf. Figure 4) for central collisions. As critically discussed by Wada et al. (2009), the reason of the disagreement between the theoretical and experimental results is still uncertain.

As a summary, both the energy needed to reach maximum filling and to fragment more than 50% of the clusters differ by one to three orders of magnitude between D&T or Ormel et al. (2009) and our simulations. The likely cause for this large discrepancy is the friction losses in our model. Our simulations do show a dramatic decrease in the total system energy due to friction, and therefore a much larger energy input is required to compact or break the clusters. Such losses could well be behind the increase by a factor of ∼1000 of the K parameter between D&T and Ormel et al.

3.6. Fragment Distributions

As a consequence of the collision process, the clusters break up and form fragments of various sizes n. We display the distribution functions $F(n)$ of fragments in Figures 10 and 11. Here $F(n)$ is the number of fragments of size n formed in the collision process. In order to reduce fluctuations, $F(n)$ is plotted as a histogram. We normalize the distributions to $F(n = 1) = 1$. These functions are interesting only beyond the agglomeration regime, starting at $v > 29v_{\rm frag}$.

We note that at the end of our simulations, the temperature of the fragments, as measured by deviations from a "local" mean velocity of grains in a cluster, was negligible. Therefore, there is no longer a role for "evaporation" of grains, and the size distribution is unchanged by running longer simulations.

Figure 10(a) discusses fragment sizes for central impacts. At the lowest velocity, $v = 29v_{\rm frag}$, a fragment with size $n \cong 2N$, survives. In addition, clusters with sizes $n = 1 \ldots 200$ are formed.

Table 1
Power Exponents τ in the Fit of the Low-fragment Size Distributions $F(n)$ to a Power Law, Equation (18)

$v/v_{\rm frag}$	$b = 0$	$b = 0.8R$	Averaged over b
29	1.97	1.92	1.78
59	1.90	1.80	1.72
118	1.99	1.94	1.73
206	2.07	3.07	2.20
353	2.40	4.78	3.10
500	3.78	5.80	5.37

With increasing velocity the large agglomerated clusters disappear; at $v = 206v_{\rm frag}$ they have vanished. For high impact velocities, the behavior for more peripheral collisions, Figure 10(b), is analogous to that of central collisions. For small velocities, however, a broader distribution of cluster sizes is obtained. In the case of the lowest impact velocity, $v = 29v_{\rm frag}$, besides cluster agglomeration with $n \cong 2N$, also intermediate cluster sizes, $10^2 < n < 10^4$, can result after the complex collision process.

Figure 11 summarizes the fragment distributions, if the collisions are averaged over the impact parameters,

$$F(n) = \frac{1}{\pi R^2} \int_{b=0}^{b=R} db 2\pi b F(n; b). \quad (17)$$

The low-size tails of the distribution, $n \lesssim 100$, can be fitted to a power-law distribution,

$$F(n) = \text{constant} \cdot n^{-\tau}. \quad (18)$$

The fits are indicated in the figures, while the exponents are given in Table 1. We see that the exponents are quite similar, $\tau \cong 2$, for small velocities ($v < 200v_{\rm frag}$ for central collisions and $v \lesssim 60v_{\rm frag}$ for more peripheral collisions). Due to the larger weight of peripheral collisions in the averaging process, Equation (17), $\tau = 2$ describes the average cluster distributions also well until $v \lesssim 200v_{\rm frag}$.

For higher velocities, the exponents increase. This is due to the fact that a large collision energy fragments the cluster in many small parts; see Figure 2(c). As noted above, the large fragment distribution, $n \gtrsim 100$ deviates systematically from the power-law distribution, Equation (18), since it is affected by the agglomeration process forming larger clusters.

These results do not agree with the picture used by Ormel et al. (2009), where fragments are fit to a power-law distribution, with a velocity-dependent exponent, plus a narrow contribution due to agglomeration. Here instead there is a wide region, above $n \sim 100$ ($\sim 0.014N$), and therefore including a significant fraction of the cluster mass, where the fragment size distribution is nearly flat. This holds for velocities below $\sim 200v_{\rm frag}$.

Paszun & Dominik (2009) studied the fragment distribution using simulations of porous clusters containing 1000 grains. They found power-law distributions which depended both on impact energy and impact parameter, but not so much on cluster filling factor (varied between 0.09 and 0.25). While for energies below $NE_{\rm break}$, the values of τ were around $2 \ldots 2.5$, τ increased strongly with energy and reached $\tau = 4$ or more for $10NE_{\rm break}$. Noting—discussed in Section 3.5 above—that the value of the break energy is different in the different models, the data given by Paszun & Dominik (2009) agree well with ours. At high impact parameters ($b = 1.5R_{\rm grain}$), Paszun & Dominik (2009) find $\tau = 2.6 \ldots 3$ for all velocities; this is somewhat discrepant with our finding (at $b = 0.8R_{\rm grain}$) that at low velocities we retain $\tau = 2$, while the increase in τ occurs at smaller velocities.

Wada et al. (2008, 2009) studied the collision of clusters (with fractal dimension 2) containing $<\sim 8000$ grains. They find fragment distributions characterized by two power laws, a steeper one for small fragments containing <10 grains and a softer decay for large fragments. They conclude that their results are in reasonable agreement with Paszun & Dominik (2009).

Ohnishi et al. (2008) used clusters with $N \sim 10^3$ and 2×10^4 atoms in their atomistic simulations, and described several regions in the fragment distribution for head-on collisions, and for the narrow, high, velocity range which they studied: $n = 1 \ldots 10$ have exponent ~ -3.75; $n = 10 \ldots 0.04N$ have an exponent ~ -1.1; and $n = 0.04 \ldots 0.1N$ have an exponent $-1 \ldots -4$, depending on cluster size and velocity. These limits would translate to $0.04N = 288$ grains, and $0.1N = 720$ grains for the case simulated here. If we note that Ohnishi et al. (2008) studied $v \sim 1.5v_{\rm sound}$, which translates to $\sim 214v_{\rm frag}$, we can directly compare the simulations of Ohnishi et al. (2008) with that of $v/v_{\rm frag} \sim 206$ in Figure 10(a), and we observe reasonably good agreement in the fragment distributions.

In the fragmentation of solid or liquid material, higher exponents are generally observed. A thermodynamic (i.e., equilibrium) model of fragmentation (Fisher 1967a, 1967b; Urbassek 1988) predicts $\tau = 7/3$ (Fisher's critical exponent) at the critical point; at other temperatures the distribution decays faster. The percolation model of fragmentation (Yarin 1993) predicts $\tau = 2.17$ at the percolation point; otherwise the fall-off is even steeper. In simulations of the fragmentation of liquid droplets upon collision with a wall (Sun & Urbassek 2011), we found exponents of $\tau \geqslant 2.38$; the smallest exponent (2.38) was found when the collision energy per molecule is around the cohesive energy of the material; for other impact energies the distributions decay faster. Large-scale computer simulation of Cu cluster impacts (diameters up to 60 nm) show fragment distributions following a power law with $\tau = 2.3$ (Germann 2006). We conclude that our results for the collision-induced fragmentation of granular clusters show a distinctly smaller power exponent than what is found for the fragmentation of non-porous condensed materials.

In a recent experiment (Güttler et al. 2010), the fragmentation distributions of granular clusters upon collision with a flat target were determined. The clusters had similar filling factors as in the present study, ranging from 0.15 to 0.35, but the clusters were considerably larger, of millimeter size. Fragment sizes (above 50 μm) were detected with a high-speed camera. For impact velocities of 1.2–8.4 m s^{-1}, a power law with an exponent of $-1.1 \ldots -1.4$ was observed; thus the distributions are significantly flatter than in our simulations, emphasizing the emission of large fragments. There may be several reasons for the disagreement with the simulation data: the camera resolution allows only detection of large fragments; the large cluster size relative to that used in simulation might be the cause that at the same impact speed relatively more large clusters are generated; the collision with a flat, hard, dense target instead of with another porous cluster. Finally we note that collision studies of asteroids, performed with SPH, demonstrate that so-called pre-fragmented

(i.e., rubble-pile) asteroids show a distinctly different fragment distribution than monolithic asteroids: large fragments sizes are enhanced and show a smaller power-law exponent (Michel et al. 2003); we state here analogies with the small exponents found for large fragments in the experiment by Güttler et al. (2010).

4. CONCLUSIONS

We presented results of collisions of loosely packed granular clusters. For clusters containing ∼7000 grains, we systematically investigated the agglomeration and fragmentation behavior in dependence of collision velocity and impact parameter. We find:

1. The regimes of sticking collisions (at low velocities and for central impacts) and of fragmentation (at higher velocities and for more peripheral impacts) show fair quantitative agreement with those found for atomic (both LJ and metallic) clusters, if the results are scaled to the respective velocities of sound.
2. Comparison with the often employed analytical model developed by Dominik & Tielens (1997) for granular collisions shows differences of more than one order of magnitude in the velocity scale. This occurs even though the decisive parameter in this model, the so-called break-up energy, is reproduced well by our simulations. This discrepancy points to the difficulties of extrapolating analytical models from nano- to micro-clusters.
3. Our results show that collision-induced compaction, which occurs in the sticking regime, is strongly inhomogeneous. While the cluster center compactifies, the outer layers remain loosely bound and porous.
4. Most interestingly, with increasing velocities, compaction first goes through a maximum and then decreases again. This is because the agglomerated clusters yield laterally to the collision pressure built up in the center. This porous layer might cushion future impacts and provide a significant surface area for astrochemistry.
5. Collisions of larger clusters (up to sizes of $N = 250{,}000$) show how the compaction behavior changes with cluster size: compaction increases both at the maximum and in particular for large velocities. This is because the clusters show more bulk-like behavior, and collision pressure can no longer so easily be relaxed laterally.
6. Fragment distributions show a power-law behavior up to fragment sizes of >100 grains. The exponent is ≈2, but changes with collision velocity and impact parameter. For larger fragments the distribution is relatively flat, as opposed to the localized agglomeration peak in Ormel et al. (2009).
7. Up to now our simulations are not yet able to properly describe thermal effects. These will be important for evaluating the thermally activated chemistry which may occur during and after collision. We are currently working on analytical and computational models to obtain improved temperature estimates, such as those included in hydrocode simulations of planetesimal collisions (Davison et al. 2010).

As a summary, we present here new results on grain–grain collisions indicating that some aspects of current models to obtain fragment size distributions might have to be re-evaluated. New experimental techniques (Hansen et al. 2011) will allow the exploration of the size and velocity ranges, which are covered in the present study and which are now still difficult to access experimentally, such that there are almost no data available.

Our simulations were targeted to silica grains, for which there is an extensive literature, but they could as well be performed for other materials found in the interstellar and interplanetary environments, provided that effects of phase change and electronic effects can be neglected. Future studies could include the collision of clusters of different sizes, of irregularly shaped clusters, or clusters including different-sized grains. Some of the complexities of core-shell structured grains (for instance silica covered with water ice) could be approached using grains with different sizes and different properties.

This work has been supported by the *Deutsche Forschungsgemeinschaft* via the Graduiertenkolleg 814. E.M.B. and D.S.B. acknowledge support from CONICET, SeCTyP (U. N. Cuyo), and PICT-2009-0092.

REFERENCES

Allen, M. P., & Tildesley, D. J. (ed.) 1987, Computer Simulation of Liquids (Oxford: Clarendon)
Anders, C., Bringa, E. M., Ziegenhain, G., et al. 2012, Phys. Rev. Lett., 108, 027601
Armitage, P. J. 2010, Astrophysics of Planet Formation (New York: Cambridge Univ. Press)
Armitage, P. J. 2011, ARA&A, 49, 195
Ashcroft, N. W., & Mermin, N. D. 1976, Solid State Physics (Philadelphia, PA: Saunders)
Asphaug, E., Agnor, C. B., & Williams, Q. 2006, Nature, 439, 155
Blum, J. 2006, Adv. Phys., 55, 881
Blum, J., & Schräpler, R. 2004, Phys. Rev. Lett., 93, 115503
Blum, J., & Wurm, G. 2000, Icarus, 148, 138
Brilliantov, N. V., Spahn, F., Hertzsch, J.-M., & Pöschel, T. 1996, Phys. Rev. E, 53, 5382
Burnham, N., & Kulik, A. A. 1999, in Handbook of Micro/Nano Tribology, ed. B. Bhushan (2nd ed.; Boca Raton, FL: CRC Press), 247
Carmona, H. A., Wittel, F. K., Kun, F., & Herrmann, H. J. 2008, Phys. Rev. E, 77, 051302
Chokshi, A., Tielens, A. G. G. M., & Hollenbach, D. 1993, ApJ, 407, 806
Cundall, P. A., & Strack, O. D. L. 1979, Géotechnique, 29, 47
Davison, T. M., Collins, G. S., & Ciesla, F. J. 2010, Icarus, 208, 468
Dominik, C., Jones, A. P., & Tielens, A. G. G. M. 1995, Astrophys. Space Sci., 233, 155
Dominik, C., & Tielens, A. G. G. M. 1997, ApJ, 480, 647
Draine, B. T., & Salpeter, E. E. 1979, ApJ, 231, 438
Ellison, D. C., Drury, L. O., & Meyer, J.-P. 1997, ApJ, 487, 197
Fisher, M. E. 1967a, Physics, 3, 255
Fisher, M. E. 1967b, Rep. Prog. Phys., 30, 615
Geretshauser, R. J., Meru, F., Speith, R., & Kley, W. 2011, A&A, 531, A166
Geretshauser, R. J., Speith, R., Güttler, C., Krause, M., & Blum, J. 2010, A&A, 513, A58
Germann, T. C. 2006, Int. J. Impact Eng., 33, 285
Güttler, C., Blum, J., Zsom, A., Ormel, C. W., & Dullemond, C. P. 2010, A&A, 513, A56
Güttler, C., Krause, M., Geretshauser, R. J., Speith, R., & Blum, J. 2009, ApJ, 701, 130
Haff, P. K., & Werner, B. T. 1986, Powder Technol., 48, 239
Hansen, J. F., van Breugel, W., Bringa, E. M., et al. 2011, J. Instrum., 6, P05010
Humphrey, W., Dalke, A., & Schulten, K. 1996, J. Mol. Graph., 14, 33
Johnson, K. L. 1985, Contact Mechanics (Cambridge: Cambridge Univ. Press)
Johnson, K. L., Kendall, K., & Roberts, A. D. 1971, Proc. R. Soc. A, 324, 301
Jones, A. P., Tielens, A. G. G. M., Hollenbach, D. J., & McKee, C. F. 1994, ApJ, 433, 797
Jutzi, M., Benz, W., & Michel, P. 2008, Icarus, 198, 242
Kalweit, M., & Drikakis, D. 2006, Phys. Rev. B, 74, 235415
Kholmurodov, K., Puzynin, I., Smith, W., Yasuoka, K., & Ebisuzaki, T. 2001, Comput. Phys. Commun., 141, 1
Kim, S.-H., Martin, P. G., & Hendry, P. D. 1994, ApJ, 422, 164
Krause, M., & Blum, J. 2004, Phys. Rev. Lett., 93, 021103
Kun, F., & Herrmann, H. J. 1996, Int. J. Mod. Phys. C, 7, 837
Kun, F., & Herrmann, H. J. 1999, Phys. Rev. E, 59, 2623
Kuninaka, H., & Hayakawa, H. 2009, Phys. Rev. E, 79, 031309

Li, A., & Greenberg, J. M. 2000, in NATO Science Series II: Mathematics, Physics and Chemistry, Vol. 120, Solid State Astrochemistry, ed. V. Pirronello, J. Krelowski, & G. Manicò (Dordrecht: Kluwer), 37
Mariscal, M. M., Dassie, S. A., & Leiva, E. P. M. 2005, J. Chem. Phys., 123, 184505
Melosh, H. J. 1989, Impact Cratering: A Geologic Process (New York: Oxford Univ. Press)
Meyers, M. A., & Chawla, K. K. 2010, Mechanical Behavior of Materials (2nd ed.; Cambridge: Cambridge Univ. Press)
Michel, P., Benz, W., & Richardson, D. C. 2003, Nature, 421, 608
Ming, L., Markovic, N., Svanberg, M., & Pettersson, J. B. C. 1997, J. Phys. Chem. A, 101, 4011
Murad, S., & Law, C. K. 1999, Mol. Phys., 96, 81
Murphy, W. J., Higginbotham, A., Kimminau, G., et al. 2010, J. Phys.: Condens. Matter, 22, 065404
Ohnishi, N., Bringa, E. M., Remington, B. A., et al. 2008, J. Phys. Chem. Solids, 112, 042017
Ormel, C. W., Paszun, D., Dominik, C., & Tielens, A. G. G. M. 2009, A&A, 502, 845
Paszun, D., & Dominik, C. 2008, A&A, 484, 859
Paszun, D., & Dominik, C. 2009, A&A, 507, 1023
Plimpton, S. 1995, J. Comput. Phys., 117, 1
Poppe, T., Blum, J., & Henning, T. 2000, ApJ, 533, 454
Pöschel, T., & Schwager, T. 2005, Computational Granular Dynamics: Models and Algorithms (Berlin: Springer)
Quesnel, D. J., Rimai, D. S., & DeMejo, L. P. 1993, Phys. Rev. B, 48, 6795
Ringl, C., & Urbassek, H. M. 2012, Comput. Phys. Commun., 183, 986
Rosenberg, Z., Bournesave, N. K., & Millett, J. C. F. 1996, J. Appl. Phys., 79, 3971
Schäfer, C., Speith, R., & Kley, W. 2007, A&A, 470, 733
Sirono, S.-i. 2004, Icarus, 167, 431
Sun, S. N., & Urbassek, H. M. 2011, Phys. Rev. E, 84, 056315
Suyama, T., Wada, K., & Tanaka, H. 2008, ApJ, 684, 1310
Svanberg, M., Ming, L., Markovic, N., & Pettersson, J. B. C. 1998, J. Chem. Phys., 108, 5888
Teiser, J., Engelhardt, I., & Wurm, G. 2011, ApJ, 742, 5
Teiser, J., & Wurm, G. 2009, MNRAS, 393, 1584
Thornton, C., & Ning, Z. 1998, Powder Technol., 99, 154
Tielens, A. G. G. M., McKee, C. F., Seab, C. G., & Hollenbach, D. J. 1987, ApJ, 319, L109
Tielens, A. G. G. M., McKee, C. F., Seab, C. G., & Hollenbach, D. J. 1994, ApJ, 431, 321
Tomsic, A., Andersson, P. U., Markovic, N., et al. 2001, J. Chem. Phys., 115, 10509
Tong, Z. B., Yang, R. Y., Yu, A. B., Adi, S., & Chan, H. K. 2009, Powder Technol., 197, 213
Urbassek, H. M. 1988, Nucl. Instrum. Methods Phys. Res. B, 31, 541
Wada, K., Tanaka, H., Suyama, T., Kimura, H., & Yamamoto, T. 2007, ApJ, 661, 320
Wada, K., Tanaka, H., Suyama, T., Kimura, H., & Yamamoto, T. 2008, ApJ, 677, 1296
Wada, K., Tanaka, H., Suyama, T., Kimura, H., & Yamamoto, T. 2009, ApJ, 702, 1490
Wada, K., Tanaka, H., Suyama, T., Kimura, H., & Yamamoto, T. 2011, ApJ, 737, 36
Weidenschilling, S. J., & Cuzzi, J. N. 1993, in Protostars and Planets III, Vol. 3, ed. E. H.Levy, J. I. Lunine (Tuscon, AZ: Univ. Arizona Press), 1031
Wurm, G., & Blum, J. 1998, Icarus, 132, 125
Wurm, G., Paraskov, G., & Krauss, O. 2005, Icarus, 178, 253
Yarin, A. L. 1993, Free Liquid Jets and Films: Hydrodynamics and Rheology (Harlow/New York: Longman/Wiley)
Zimmermann, S., & Urbassek, H. M. 2006, Phys. Rev. A, 74, 063203
Zsom, A., Ormel, C. W., Güttler, C., Blum, J., & Dullemond, C. P. 2010, A&A, 513, A57